JBC RESEARCH ARTICLE

Mitochondrial glutathione peroxidase 4 is indispensable for photoreceptor development and survival in mice

Received for publication, January 21, 2022, and in revised form, March 3, 2022 Published, Papers in Press, March 11, 2022,
https://doi.org/10.1016/j.jbc.2022.101824

Kunihiro Azuma[1], Tomoko Koumura[2], Ryo Iwamoto[2], Masaki Matsuoka[2], Ryo Terauchi[3,4], Shu Yasuda[2], Tomoyasu Shiraya[1], Sumiko Watanabe[3], Makoto Aihara[1], Hirotaka Imai[2,*], and Takashi Ueta[1,*]

From the [1]Department of Ophthalmology, Graduate School of Medicine, The University of Tokyo, Tokyo, Japan; [2]Department of Hygienic Chemistry and Medical Research Laboratories, School of Pharmaceutical Sciences, Kitasato University, Tokyo, Japan; [3]Division of Molecular and Developmental Biology, Institute of Medical Science, The University of Tokyo, Tokyo, Japan; [4]Department of Ophthalmology, The Jikei University School of Medicine, Tokyo, Japan

Edited by Phyllis Hanson

Glutathione peroxidase 4 (GPx4) is known for its unique function in the direct detoxification of lipid peroxides in the cell membrane and as a key regulator of ferroptosis, a form of lipid peroxidation–induced nonapoptotic cell death. However, the cytosolic isoform of GPx4 is considered to play a major role in inhibiting ferroptosis in somatic cells, whereas the roles of the mitochondrial isoform of GPx4 (mGPx4) in cell survival are not yet clear. In the present study, we found that mGPx4 KO mice exhibit a cone–rod dystrophy-like phenotype in which loss of cone photoreceptors precedes loss of rod photoreceptors. Specifically, in mGPx4 KO mice, cone photoreceptors disappeared prior to their maturation, whereas rod photoreceptors persisted through maturation but gradually degenerated afterward. Mechanistically, we demonstrated that vitamin E supplementation significantly ameliorated photoreceptor loss in these mice. Furthermore, LC–MS showed a significant increase in peroxidized phosphatidylethanolamine esterified with docosahexaenoic acid in the retina of mGPx4 KO mice. We also observed shrunken and uniformly condensed nuclei as well as caspase-3 activation in mGPx4 KO photoreceptors, suggesting that apoptosis was prevalent. Taken together, our findings indicate that mGPx4 is essential for the maturation of cone photoreceptors but not for the maturation of rod photoreceptors, although it is still critical for the survival of rod photoreceptors after maturation. In conclusion, we reveal novel functions of mGPx4 in supporting development and survival of photoreceptors *in vivo*.

Glutathione peroxidase 4 (GPx4) is a ubiquitously expressed antioxidant enzyme with a unique function that directly reduces peroxidized phospholipids in the cell membrane. GPx4 is known as a critical regulator of ferroptosis (1), lipid peroxidation–induced nonapoptotic cell death, and indispensable for development and survival. A conventional KO of GPx4 in mice leads to early embryonic death (2). Conditional KO of GPx4 in the heart and liver has been shown to cause embryonic and neonatal death, respectively (3, 4), whereas loss of GPx4 specifically in spermatocytes causes male infertility (5). Furthermore, tamoxifen-induced GPx4 KO is known to cause acute renal failure and death (6).

GPx4 consists of three isoforms; mitochondrial (mGPx4), nucleolar (nGPx4), and cytosolic (cGPx4), which are located at the mitochondria, nucleolus, and the other subcellular spaces, respectively (7, 8). In somatic tissues and cultured cells, cGPx4 is considered dominantly expressed relative to mGPx4 and nGPx4 (9). In addition, cGPx4 KO mice die embryonically, whereas mGPx4 or nGPx4 KO does not affect development and survival, except for male infertility in mGPx4 KO mice (3, 10). In addition, the lethality caused by total GPx4 KO can be rescued by cGPx4 but not by mGPx4 or nGPx4 (3, 11, 12). These observations have suggested that cGPx4 is the key isoform for survival, whereas the role of mGPx4 is not yet fully understood.

Photoreceptors, consisting of cones and rods, play pivotal roles in the visual system by cooperating with retinal pigment epithelium (RPE). Rod photoreceptors specialize in scotopic vision and have low spatial acuity; cone photoreceptors specialize in photopic color vision and have high spatial acuity. Polyunsaturated fatty acids (PUFAs), especially docosahexaenoic acid (DHA), are highly concentrated at the outer segments of photoreceptors and are vulnerable to oxidative stress (13, 14). In addition, photoreceptors are also known to have the highest levels of energy demand and production through oxidative metabolism in mitochondria located exclusively at the inner segment of photoreceptors (15). We previously reported that conditional KO of all GPx4 isoforms in photoreceptors in mice led to early degenerative phenotypes, revealing the importance of GPx4 for the survival of photoreceptors (16). In the present study, to further elucidate the isoform-specific roles of GPx4, we evaluated the eyes of mGPx4 KO mice. Unexpectedly, we found a phenotype of retinal degeneration in which both cone and rod photoreceptors were affected but with different severities and at different developmental stages. Thus, our findings provide insights into previously undetermined roles of mGPx4.

* For correspondence: Takashi Ueta, ueta-tky@umin.ac.jp; Hirotaka Imai, imaih@pharm.kitasato-u.ac.jp.

Results

Generation of mGPx4 KO mice

We previously generated GPx4 heterozygous mice ($GPx4^{+/-}$) by homologous recombination with a PGK-Neo cassette (2), and the embryonic lethality of GPx4 KO mice was rescued by loxP-GPx4 transgene that expresses all isoforms of GPx4 ($GPx4^{-/-}$::$GPx4^{tg(loxP\text{-}GPx4)/tg(loxP\text{-}GPx4)}$, Fig. S1*A*) (9, 12, 16). For this study, mGPx4 KO mice ($GPx4^{-/-}$::$GPx4^{tg(mGPx4\ KO)/tg(mGPx4\ KO)}$) were generated in which the lethality of GPx4 KO was rescued by mGPx4 KO transgene (Fig. S1, *A* and *B*) that expresses cGPx4 and nGPx4 but lacks mGPx4. Indeed, Western blot analysis on fractionated samples of the testis confirmed that GPx4 expression was abrogated in the mitochondria, whereas maintained in the cytosol and nucleus in mGPx4 KO mice (Fig. S1*C*). In contrast, littermate $GPx4^{+/-}$::$GPx4^{tg(mGPx4\ KO)/tg(mGPx4\ KO)}$ mice in which potential defects in mGPx4 KO mice are rescued by a wild allele of GPx4 were used as control mice.

mGPx4 deficiency leads to retinal degeneration

To confirm specific mGPx4 deficiency in the retina, cytosolic and mitochondrial fractions of the retina were prepared and analyzed on Western blot (Fig. 1*A*). Expectedly, in mGP4 KO retina, GPx4 was not detected in the mitochondrial fraction, whereas the levels of GPx4 in the cytosol were similar to those in WT and control retina (Fig. 1, *A* and *B*). Immunohistochemistry of mGPx4 KO retina showed that GPx4 expression is severely downregulated in the inner segments of photoreceptors where mitochondria are condensed (Fig. 1*C*). On fundus photographs, the mGPx4 KO mouse at 3 months old presented with pigmentation, retinal vascular narrowing, and optic atrophy compared with the control mouse retina (Fig. 1*D*). Acrolein, a product of lipid peroxidation, was upregulated in the mGPx4 KO mouse retina at P14 compared with in the control mouse retina (Fig. 1*E*). Hematoxylin–eosin staining revealed a progressive degeneration after P7 in photoreceptors that locate at the outer nuclear layer (ONL; Fig. 1*F*). In detail, rod photoreceptors expressing rhodopsin survived at least until P30, whereas cone photoreceptors labeled with peanut agglutinin (PNA) were not observed as early as P7 (Fig. 1*G*). On RPE flatmounts, RPE cells did not show degeneration, confirming that the degeneration originates from the photoreceptors themselves and is not secondary to RPE degeneration (Fig. 1*H*).

Vitamin E partially rescues photoreceptor death caused by mGPx4 deficiency

Previous studies have shown that a vitamin E (vit E)-enriched diet rescues cell death caused by GPx4 ablation *in vitro* and *in vivo* (3–5, 17–20), through its effect of preventing lipid peroxidation (21). To examine the rescue effect of vit E in relation to mGPx4-deficient retinas, maternal mice were fed on a vit E-enriched diet (1000 IU/kg) from late pregnancy to the end of the experiments, through which the offspring were also supplemented with vit E. We found that the ONL of vit E-supplemented mGPx4 KO mice was significantly thicker than the ONL of mice fed on a normal diet (Fig. 2, *A* and *B*). The number of TUNEL-positive dead cells in the ONL significantly increased in mGPx4 KO mice fed on a normal diet, and this effect was significantly rescued by vit E supplementation (Fig. 2, *A* and *C*).

Next, we addressed the effects of mGPx4 KO and vit E supplementation in cone photoreceptors that were affected more severely than rods. The expression of s-opsin, a marker of mature cone photoreceptors, was not observed in mGPx4 KO mice, and the rescue effect by vit E supplementation was relatively small, although statistically significant (Fig. 2, *D* and *E*). Similarly, the expression of cone arrestin, another marker of mature cone photoreceptors, was not observed in the mGPx4 KO retina, and vit E supplementation did not show a significant rescue effect (Fig. 2*D*). In contrast, the expression of Rxr-γ, a specific marker of cone photoreceptor precursor, was favorably expressed at P0 in the retina of mGPx4 KO mice, although it disappeared by P7. Vit E supplementation postponed the loss of cone precursors and significantly increased the number of Rxr-γ-positive photoreceptors at P4 (Fig. 2, *F* and *G*). These results indicate that detoxifying peroxidized phospholipids in mitochondria are essential for the development of cone photoreceptors. However, rod photoreceptors can develop to their mature stage without mGPx4, although mGPx4 KO causes rod photoreceptor death at a later stage.

To further clarify the differences in the effects of mGPx4 deficiency between cone and rod photoreceptors, electroretinogram (ERG) evaluations were performed (Fig. 3). The amplitude of both a-waves and b-waves of the scotopic condition was significantly lower in mGPx4 KO mice at 7 weeks old compared with the control mice (Fig. 3, *A*–*C*). In vit E-supplemented mGPx4 KO mice, the amplitude of both a-waves and b-waves was significantly higher than that in mGPx4 KO mice without vit E supplementation. In the photopic condition evaluated in 4-week-old mice, the amplitude of both a-waves and b-waves was significantly lower in mGPx4 KO mice than that in control mice. Vit E supplementation did not confer rescue effects on both photopic a-waves and b-waves (Fig. 3, *D*–*F*), which was consistent with our histology data (shown in Fig. 2, *D*–*G*). These results indicate that vit E ameliorates dysfunction in rod photoreceptors but not in cone photoreceptors. In addition, together with our histologic findings (Figs. 1 and 2), mGPx4 KO mice recapitulate some of the key features for human cone–rod dystrophy.

Mitochondrial abnormality in the photoreceptors of mGPx4 KO mice

To further investigate the roles of mGPx4, the retina at P17 was examined using transmission electron microscopy (TEM). Longitudinal sections of the mitochondria in the inner segments of mGPx4 KO mouse photoreceptors revealed that the number of mitochondria was significantly decreased and that the area per mitochondrion was significantly increased relative to equivalent observations in control mice (Fig. 4, *A*–*C*). The results suggest the occurrence of mitochondrial fusion because of mitochondrial oxidative stress caused by mGPx4 deficiency. Therefore, proteins related to mitochondrial fusion/fission

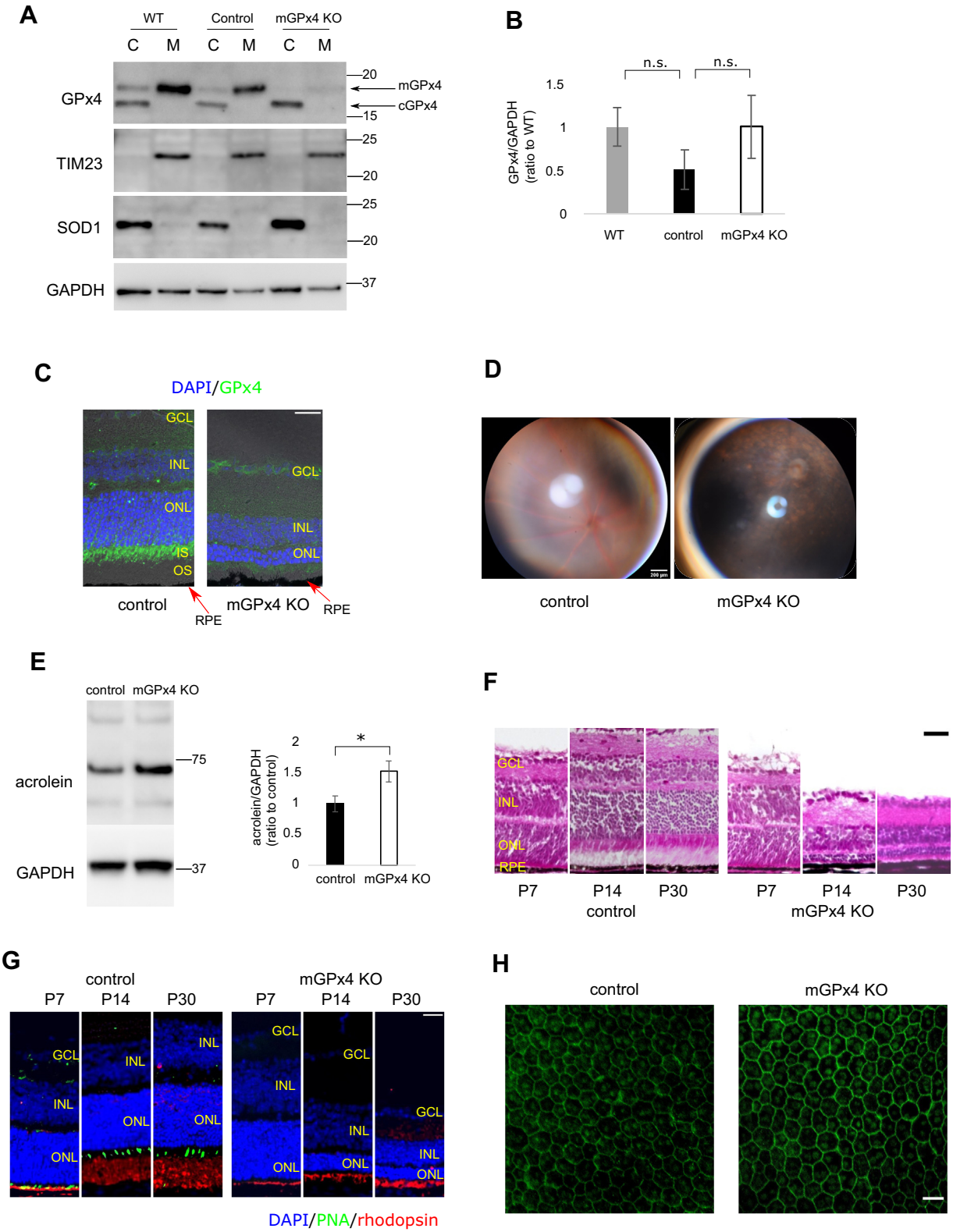

Figure 1. Photoreceptor degeneration in mGPx4 KO mouse retina. *A*, Western blots of cytosolic (C) and mitochondrial (M) fractions of the retina from WT, control, and mGPx4 KO mice. TIM23 and SOD1 served as mitochondrial and cytosolic markers, respectively. mGPx4 was detected in samples from WT and control retina but not in samples from mGPx4 KO retina. *B*, quantification of cGPx4 levels in cytosol fraction, indicating retained cGPx4 levels in mGPx4 KO mouse retina (n = 4 per group). Analysis was performed using one-way ANOVA and the Tukey–Kramer post hoc test. *C*, GPx4 expression in the retina of control and mGPx4 KO mice. Higher GPx4 levels were observed in inner segments in control mouse where mitochondria are condensed, which was not observed in mGPx4 KO mice (consistent in three independent samples per group). *D*, color fundus photographs of control and mGPx4 KO mice. Pigmentation, retinal vascular narrowing, and optic atrophy were observed in the fundus of mGPx4 KO mice (consistent in three independent samples per group). *E*, mGPx4 KO mouse retina contained more acrolein derived from lipid peroxidation than control retina on Western blot analysis (n = 6 per group). *F*, hematoxylin–eosin staining showed thinner ONL in mGPx4 KO mouse at P14 and P30 (consistent in three independent samples per group).

were evaluated by Western blotting. Levels of the mitochondrial fusion protein mitofusion 2 (MFN2) were significantly higher in the mGPx4 KO mouse retina compared with in the control mouse retina (Fig. 4*D*). Consistently, transverse sections of the mitochondria using TEM revealed frequent mitochondrial fusions in mGPx4 KO photoreceptors, whereas it was not observed in control mice (Fig. 4*E*). In contrast, there was no significant difference in the levels of other fusion/fission proteins, such as optic atrophy 1, mitofusion 1 (MFN1), phosphorylation of dynamin-related protein 1 (DRP1), at Ser616 and Ser637 (Fig. S2). In a recent study, it was reported that mitochondria in healthy photoreceptor inner segments align with those of neighboring inner segments across plasma membranes (22). Such mitochondrial alignment was confirmed in our control mice, whereas it disorganized in mGPx4 KO mice (Fig. 4*E*).

Apoptotic photoreceptor death in mGPx4 KO mice

As the photoreceptor death was caused by mGPx4 KO, the subcellular morphology of photoreceptors was investigated using TEM; uniformly dense and shrunk pyknotic nuclei were observed in the ONL of P17 mGPx4 KO mice, but not in that of the control (Fig. 5, *A* and *B*), indicating apoptotic cell death (23). The results were further supported by the detection of caspase-3 activation in the photoreceptors of mGPx4 KO mice that was suppressed by vit E (Fig. 5*C*).

Peroxidized phosphatidylethanolamine (22:6/22:6) in mGPx4 KO retinas

PUFA-associated phospholipids are vital for photoreceptors' physiological functions and survival. To assess the effects of mGPx4 ablation on PUFA-associated phospholipids, LC–MS was used to compare phosphatidylethanolamine (PE) and phosphatidylcholine (PC), the two major phospholipids in mitochondria (24), among the retinas from the control, mGPx4 KO, and vit E-supplemented mGPx4 KO mice at P10, that is, the early phase of photoreceptor degeneration (Fig. 6). The concentrations of unchanged forms of PE-PUFAs tended to be lower in mGPx4 KO retinas than in the control and vit E-supplemented mGPx4 KO retinas. Specifically, the relative concentration of PE (22:6/22:6), which contains two chains of DHA, was significantly lower in mGPx4 KO retinas than in control and vit E-supplemented mGPx4 KO retinas (Fig. 6*A*). Accordingly, peroxidized PE (22:6/22:6-OOH) concentration was significantly increased in mGPx4 KO mouse retinas compared with the PE (22:6/22:6-OOH) concentration in control and vit E-supplemented mGPx4 KO mouse retinas (Fig. 6*B*). PE (18:0/22:6-OOH) concentration also tended to be higher in mGPx4 KO retinas, but this effect was not statistically significant. There was no significant difference in hydroxy PE-PUFAs, the reduced form of peroxidized PE-PUFAs, among the three groups (Fig. 6*C*). For PC-PUFAs, there was a tendency for unchanged forms of PC-PUFAs to decrease (Fig. 6*D*) and hydroxy PC-PUFAs to increase (Fig. 6*F*), although not at statistically significant levels.

Spermatozoa abnormalities in mGPx4 KO mice

As already shown in a previous study (10), our mGPx4 KO mice also presented with male infertility and abnormal spermatozoa. Mitochondria in the midpiece of the spermatozoa were swollen in mGPx4 KO mice (Fig. S3*A*). Flagella of mGPx4 KO spermatozoa were bent into hairpin-like shape (Fig. S3*B*), and mitochondrial membrane potential of mGPx4 KO spermatozoa was significantly lower (Fig. S3*C*). Vit E treatment rescued the mitochondrial membrane potential (Fig. S3*C*) but was not effective to mitigate the bent flagella (Fig. S3*B*) or male infertility, suggesting a redox-independent role of mGPx4 in the spermatozoa. No apparent abnormality was observed in the seminiferous tubules of mGPx4 KO mice (Fig. S3*D*), and there was no difference in the number of spermatozoa between mGPx4 KO and WT mice (Fig. S3*E*). In contrast, our previous study revealed that spermatocyte-specific KO of all isoforms of GPx4 in mice displayed a dramatic loss in the number of spermatocyte and spermatozoa in the testis (5), suggesting that mGPx4 is critically important for the fertilization of spermatozoa, while may be dispensable for the synthesis and/or survival of spermatozoa.

Discussion

GPx4 is crucial for the development and survival of numerous types of cells. However, the isoform-specific roles of GPx4 are still obscure. This study and studies by other researchers have shown that mGPx4 KO mice grow normally but exhibit male infertility because of defective sperm motility and abnormal tail structure (10, 11). To date, in the somatic tissues, cGPx4 has been believed to be more dominantly expressed than mGPx4, and mGPx4 dominance in the testis has been considered to be exceptional (10). Our data show that mGPx4 is predominant in photoreceptors.

We have previously reported that the loss of all isoforms of GPx4 in photoreceptors led to rapid cell death (16); however, the isoform-specific roles of GPx4 in photoreceptors were not addressed. The present study reveals the pivotal role of mGPx4 in photoreceptor survival *in vivo*. In contrast to other somatic cells in which cGPx4 is more dominant than mGPx4 (10), our data show that mGPx4 is predominant in photoreceptors. However, cGPx4 still might also contribute to photoreceptor survival because photoreceptor degeneration observed in mGPx4 KO mice was milder than that observed in photoreceptors lacking all isoforms of GPx4 (16).

G, immunohistochemistry for rhodopsin-expressing rod and PNA-stained cone photoreceptors. In mGPx4 KO mouse retina, cone photoreceptors were not present at P7, P14, or P30. Some of the rod photoreceptors remained in existence at least until P30 (consistent in three independent samples per group). *H*, immunohistochemistry of RPE flatmounts using anti-ZO-1 antibody in control and mGPx4 KO mouse at P14. No apparent degeneration was observed in the RPE of mGPx4 KO mice (consistent in three independent samples per group). All scale bars are 25 μm except one in (*D*), which is 200 μm. $*p < 0.05$, $**p < 0.01$ (KO with vitamin E *versus* KO), $\#p < 0.05$, $\#\#p < 0.01$ (KO *versus* control) using Student's *t* test for two-group comparison and one-way ANOVA and the Tukey–Kramer post hoc test for three-group comparison. mGPx4, mitochondrial isoform of GPx4; ONL, outer nuclear layer; PNA, peanut agglutinin; RPE, retinal pigment epithelium; SOD1, super dismutase 1.

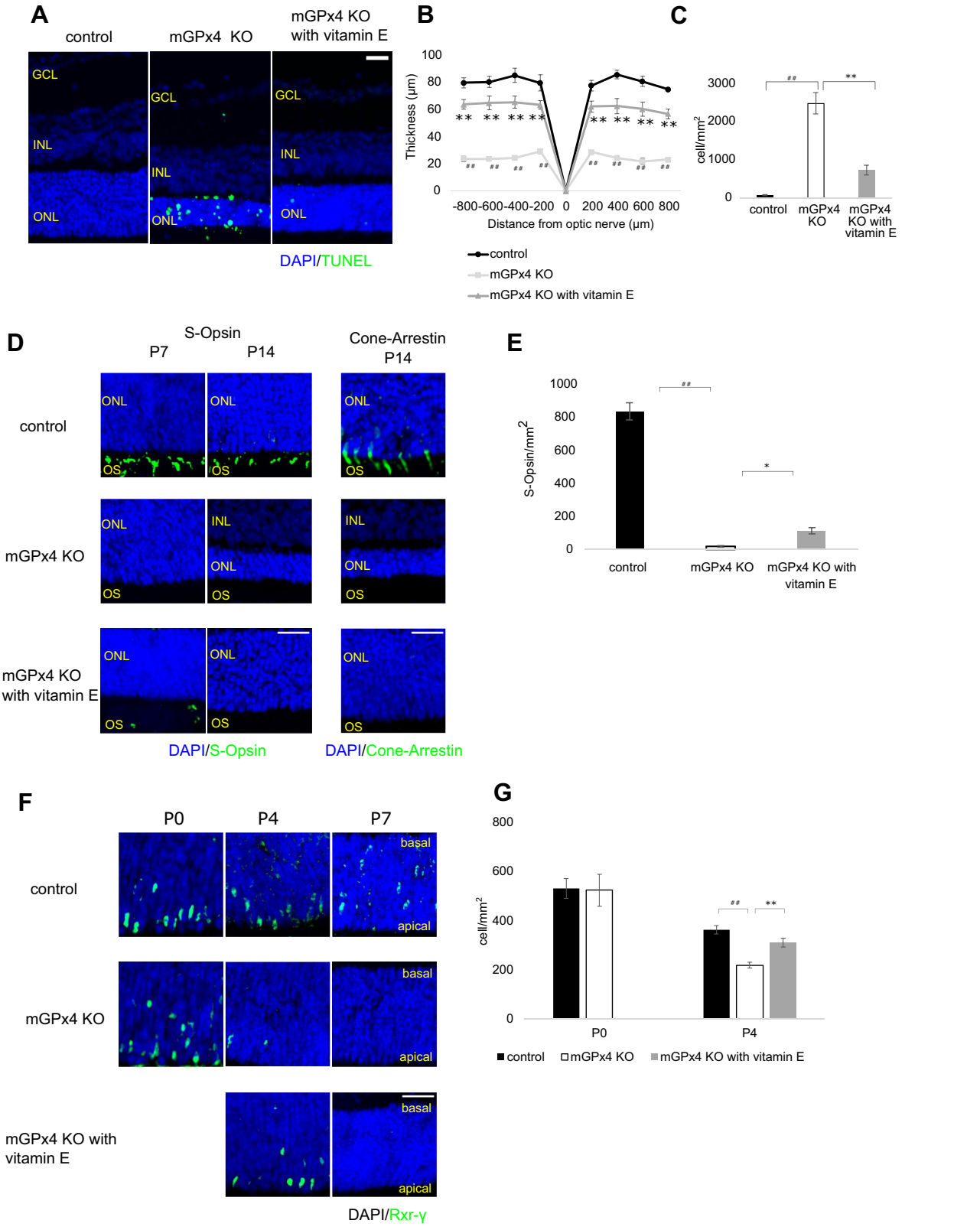

Figure 2. Vitamin E supplementation ameliorated retinal degeneration in mGPx4 KO mice. *A*, TUNEL staining of the retinas in control, mGPx4 KO, and vit E-supplemented mGPx4 KO mice at P14. *B*, ONL thickness at P14 in control, mGPx4 KO, and vit E-supplemented mGPx4 KO mice. The ONL of mGPx4 KO mouse retina was significantly thinner than control mouse retina, which was partially rescued by vit E supplementation (n = 4–5 in each group). *C*, a significantly larger number of TUNEL-positive photoreceptors were detected in mGPx4 KO mouse retina than in control at P14, which was partially rescued by vit E supplementation (n = 6 per group). *D*, immunohistochemistry for cone-specific marker s-opsin and cone arrestin. S-opsin expression was not detectable in mGPx4 KO mice at P7 and P14. Vit E supplementation mildly rescued the s-opsin expression at P7 but not at P14. Cone–arrestin expression was not observed in mGPx4 KO or vit E-supplemented mGPx4 KO mice at P14. *E*, quantification for the number of s-opsin-expressing outer segments of cone photoreceptors in control, mGPx4 KO, and vit E-supplemented mGPx4 KO mice (n = 8 per group). *F*, immunohistochemistry for cone precursor marker

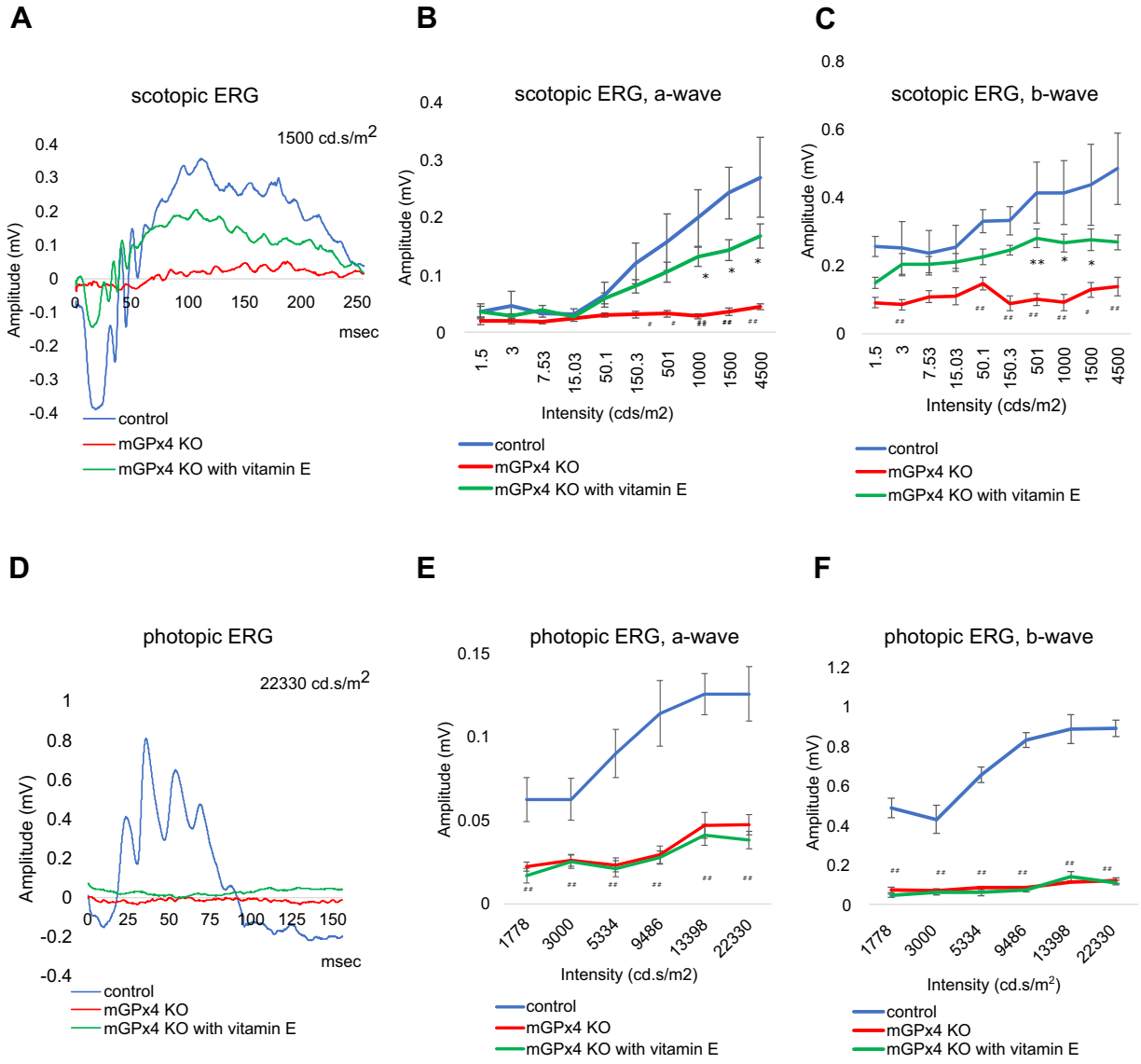

Figure 3. Functional abnormalities in mGPx4 KO mouse retina on electroretinogram. *A*, representative scotopic ERG in 7-week-old mice. *B* and *C*, in scotopic condition, the amplitude of both a-wave and b-wave was significantly diminished in mGPx4 KO mice, which was partially rescued by vit E supplementation (n = 3, 5, and 6 for control, mGPx4 KO, and vit E-supplemented mGPx4 KO). *D*, representative photopic ERG in 4-week-old mice. *E* and *F*, in photopic condition, the amplitude of both a-wave and b-wave was totally lost in mGPx4 KO mice, which could not be rescued by vit E supplementation (n = 6 for control and mGPx4 KO, n = 8 for vit E-supplemented mGPx4 KO). *$p < 0.05$, **$p < 0.01$ (KO with vitamin E *versus* KO), #$p < 0.05$, ##$p < 0.01$ (KO *versus* control) using one-way ANOVA and the Tukey–Kramer post hoc test. ERG, electroretinogram; mGPx4, mitochondrial isoform of GPx4; vit E, vitamin E.

The central nervous system, including brain and retina, consumes 20% of total oxygen and a quarter of total glucose used for energy supply; indeed, the retina ranks among the highest of the energy-consuming tissues in the central nervous system (15). The retina consists of different types of neural and glial cells. The expression of energy-generating cytochrome *c* oxygenase as well as energy-consuming Na^+/K^+-ATPase is the highest in the inner segments of the photoreceptors (15). Moreover, compared with rod photoreceptors, cone photoreceptors contain a significantly higher mitochondrial volume of mitochondria; hence, they produce more metabolic energy (15). In the mGPx4 KO mouse retina, damage was most severe in the cone photoreceptors and less severe in the rod photoreceptors. Therefore, the severity of degenerations among the different cell types of mGPx4 KO mouse retina was correlated with the levels of physiological energy demands. In contrast, vit E supplementation was able to rescue rod photoreceptors morphologically and functionally, whereas cone photoreceptors could not survive after P7 even with vit E supplementation. These results indicate that cone photoreceptors may be

Rxr-γ. Rxr-γ expression levels were similar between control and mGPx4 KO mouse retina at P0 but diminished at P4 and P7 in mGPx4 KO mice. Rxr-γ expression was restored in vit E-supplemented mGPx4 KO mice at P4 but not at P7. *G*, quantification for the number of Rxr-γ-expressing cells at P0 and P4 (n = 12 per group). All scale bars represent 25 μm. *$p < 0.05$, **$p < 0.01$ (KO with vitamin E *versus* KO), #$p < 0.05$, ##$p < 0.01$ (KO *versus* control) using one-way ANOVA and the Tukey–Kramer post hoc test. mGPx4, mitochondrial isoform of GPx4; ONL, outer nuclear layer; vit E, vitamin E.

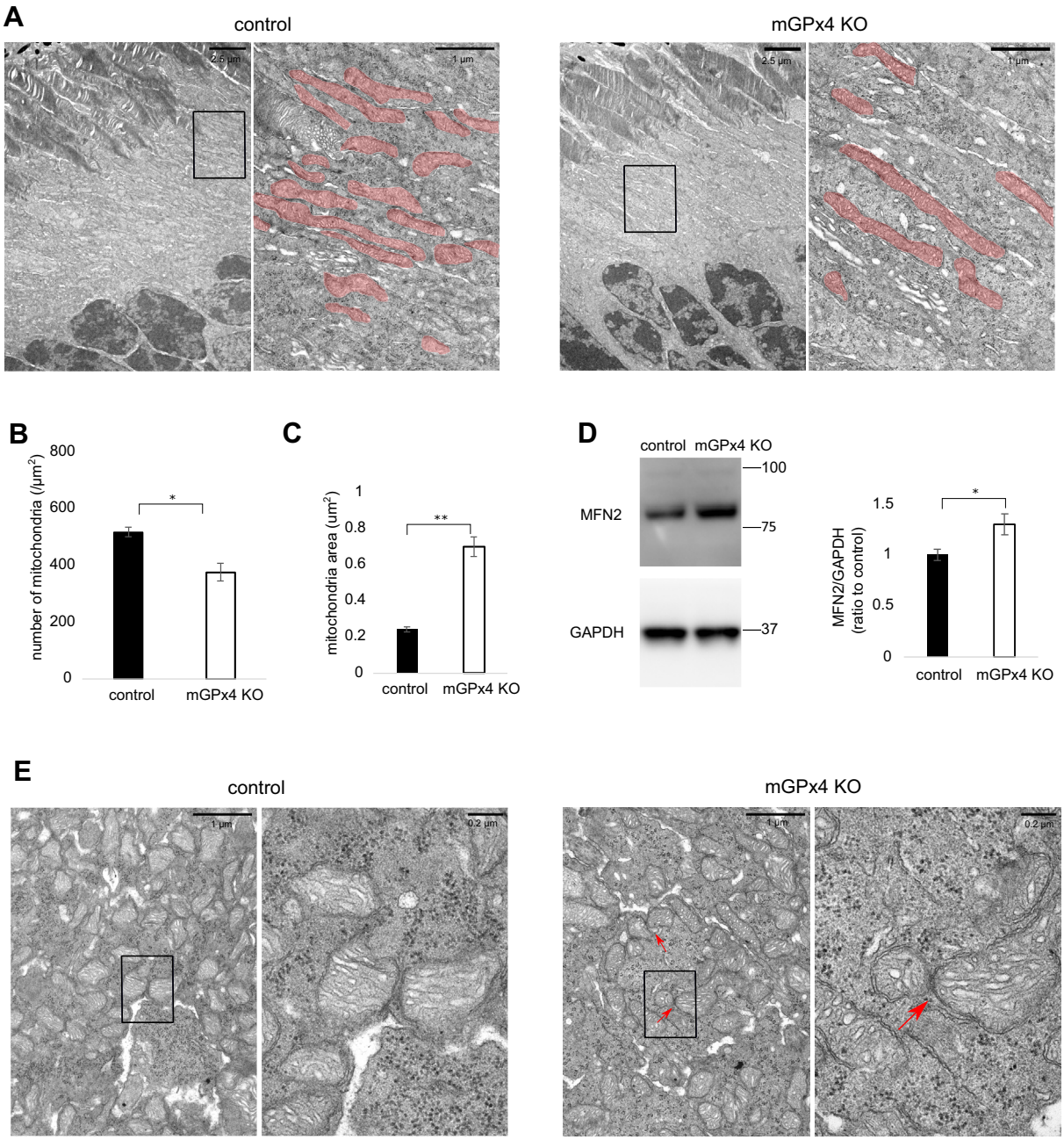

Figure 4. Mitochondrial abnormalities in mGPx4 KO mouse photoreceptors. *A*, representative transmission electron microscopy (TEM) images of longitudinal sections of inner segments of photoreceptors at P17. Areas inside the enclosing frames in the *left* (the scale bars represent 2.5 μm) are shown magnified in the *right* (the scale bars represent 1 μm). Mitochondria were marked with *red shadows*. In photoreceptor inner segments of control mice, mitochondria of neighboring photoreceptors align with close association. In contrast, such physiological mitochondrial alignment was disrupted in mGPx4 KO mouse photoreceptors (representatives of three independent samples per group). *B*, the smaller number of mitochondria was observed in photoreceptor inner segments of mGPx4 KO mice compared with those of control mice on TEM (the number of mitochondria per 23.5 μm^2 area of inner segments, n = 4 per group). *C*, area of each mitochondrion in photoreceptor inner segments was larger in mGPx4 KO compared with control mice on TEM (n = 3 per group, each value was the representative of >30 mitochondria). *D*, Western blot analysis indicated higher MFN2 expression in mGPx4 KO than in control mice (n = 6 per group). *$p < 0.05$, **$p < 0.01$ using Student's *t* test. *E*, representative TEM images of transverse sections of inner segments of photoreceptors at P17 in control and mGPx4 KO mice. Areas inside the enclosing frames in the *left* (the scale bars represent 1 μm) are shown magnified in the *right* (the scale bars represent 0.2 μm). Mitochondrial fusions (*red arrows*) were observed in mGPx4 KO mice and not in control mice (consistent in three independent samples per group). MFN2, mitofusion 2; mGPx4, mitochondrial isoform of GPx4.

more vulnerable to lipid peroxidation in mitochondria than rods, which is consistent with previous studies highlighting the pathogenic role of oxidative stress, particularly in the loss of cone photoreceptors in retinal degeneration (25, 26). However, it remains unclear whether the photoreceptor degenerations were caused directly by mitochondrial lipid peroxidation in photoreceptors or indirectly by changes in other cell types because mGPx4 was deficient in whole body of the mGPx4 KO mice. The considerable difference in the rescue effects by vit E for cone and rod photoreceptors might be explained by the limited transfer of vit E through placenta (27) and the fact that the differentiation into cone photoreceptors takes place before

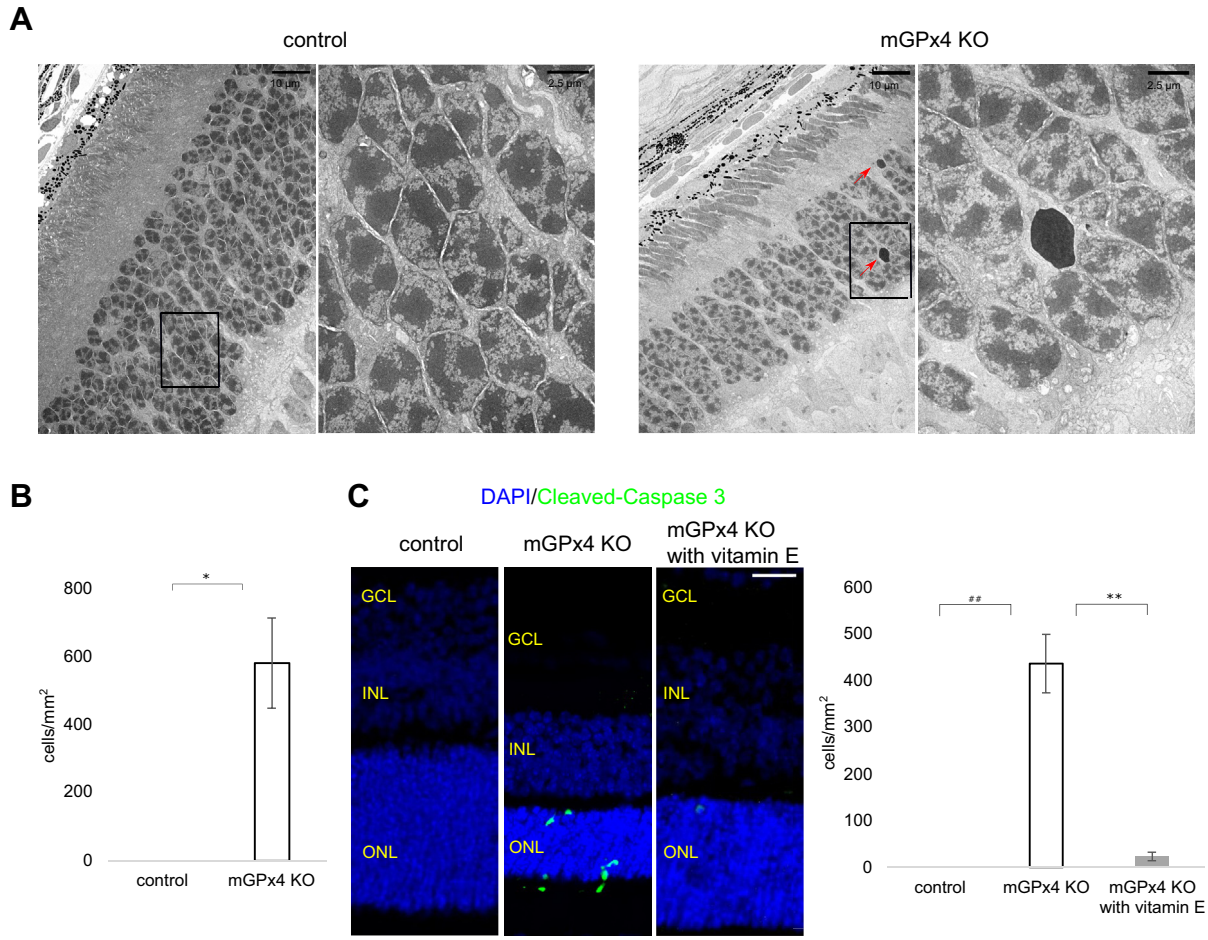

Figure 5. Apoptosis of photoreceptors in mGPx4 KO mice. *A*, in the ONL of P17 mGPx4 KO mouse retina, TEM disclosed the presence of uniformly dense and shrunk pyknotic nuclei (*red arrows*), which was not observed in control mouse retina. Areas inside the enclosing frames in the *left* (the scale bars represent 10 μm) are shown magnified in the *right* (the scale bars represent 2.5 μm). *B*, quantification of the apoptotic nuclei observed in TEM images in control and mGPx4 KO mice (n = 3 for control, n = 5 for mGPx4 KO; three views per sample). *$p < 0.05$ (KO *versus* control) using Student's *t* test. *C*, immunohistochemistry for cleaved-caspase 3 confirmed caspase activation in photoreceptors of mGPx4 KO mice. Vit E treatment decreased the number of cleaved-caspase 3-positive cells in mGPx4 KO mice (the scale bar represent 25 μm). **$p < 0.01$ (KO with vit E *versus* KO), #$p < 0.05$, ##$p < 0.01$ (KO *versus* control) using one-way ANOVA and the Tukey–Kramer post hoc test. n = 3 per group and three views per sample. mGPx4, mitochondrial isoform of GPx4; ONL, outer nuclear layer; TEM, transmission electron microscopy; Vit E, vitamin E.

birth while the differentiation into rod photoreceptors occurs just after birth. Therefore, the levels of exposure to vit E may differ between cone and rod photoreceptors in their early developmental phases (28). In contrast, previous studies have indicated that GPx4 might function as a structural protein, independent of detoxifying peroxidized lipids, in the mitochondria of spermatocytes (5, 29), which might also be the reason why vit E supplementation resulted in the partial rescue of photoreceptors in mGPx4 KO mice.

An omega-3 PUFA DHA is one of the major long-chain PUFAs in the retina and rod outer segment membranes (13, 14); it is critically important for the maintenance of photoreceptors and their survival (30). Furthermore, photoreceptors are known to contain unique phospholipids harboring two omega-3 PUFAs esterified at both sn-1 and sn-2 positions of the glycerol backbone (31), which was also confirmed in the present study. Previous studies have elucidated the key roles played by PUFAs esterified to PE (*i.e.*, PE-PUFAs) in lipid peroxidation and ferroptosis (32). Consistently, in mGPx4 KO mouse retinas, we observed a significant increase in the level of PE (22:6/22:6-OOH), but no significant change in PC-PUFAs. In addition, vit E supplementation suppressed the increase in peroxidized PE-PUFAs and ameliorated the degenerative phenotypes both anatomically and functionally. However, our observations by TEM revealed that the size of each mitochondria in mGPx4 KO mouse photoreceptors was larger, which is not typical for ferroptosis in which mitochondria are smaller (33–35). In addition, we also observed uniformly dense and shrunk pyknotic nuclei, as well as caspase-3 activation in mGPx4 KO mouse photoreceptors, suggesting the existence of apoptotic cells at least in part. In typical ferroptosis, the morphology of nuclei remains intact (36). Our observations are consistent with previous *in vitro* studies showing that mGPx4 overexpression suppressed cytochrome *c* release and caspase activation and rescued cell death induced by apoptosis inducers, including staurosporine, 2-deoxyglucose, and Fas-specific antibodies (37, 38).

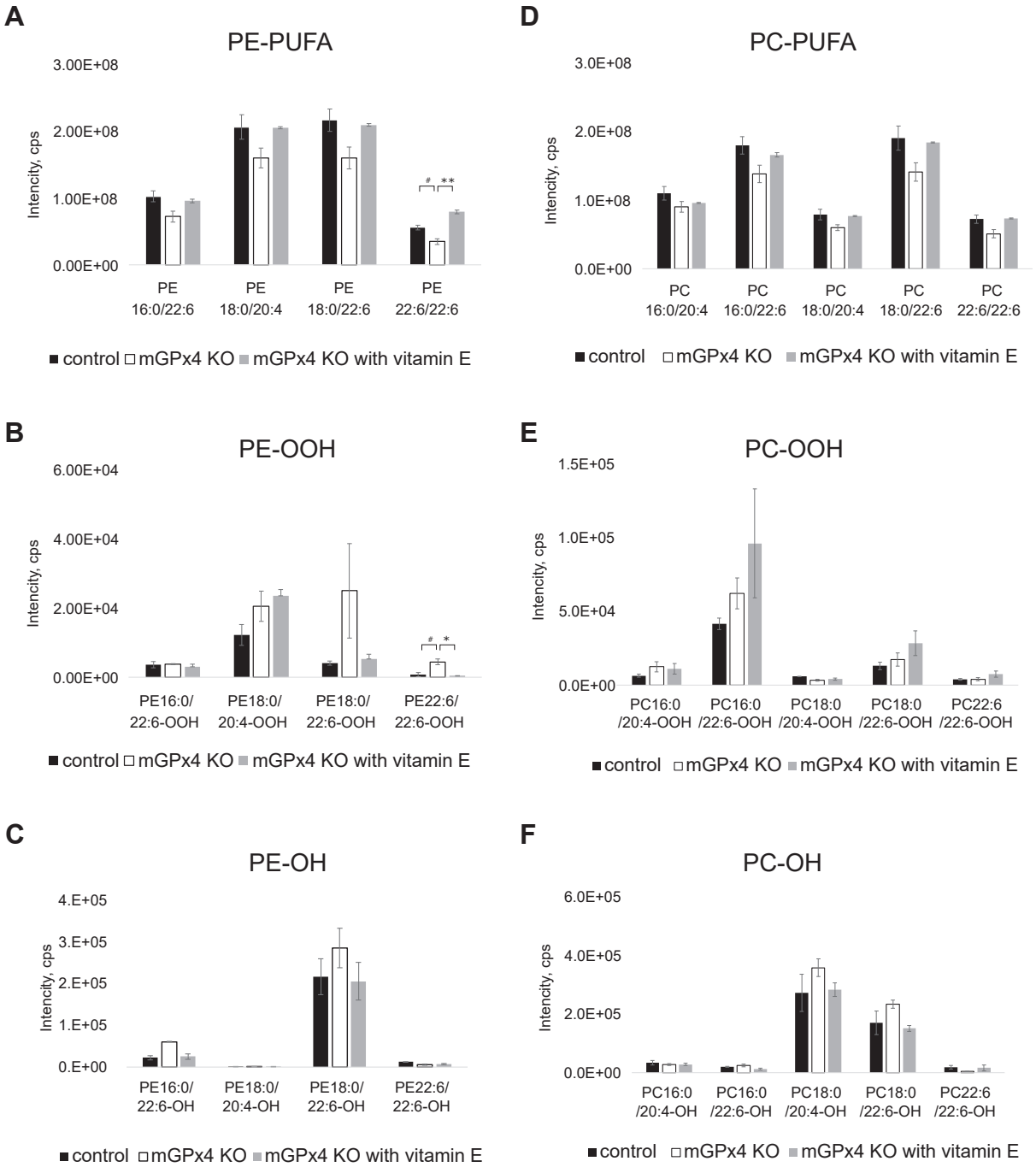

Figure 6. LC–MS analysis indicated increased phospholipid peroxidation of PE 22:6/22:6 in mGPx4 KO mice retina. *A*, PE 22:6/22:6 (DHA esterified at both sn-1 and sn-2 positions of PE) was significantly decreased in mGPx4 KO mice retina at P10 compared with control, which was blocked by vit E supplementation (n = 3 per group). *B*, peroxidized PE 22:6/22:6-OOH was significantly increased in mGPx4 KO mice at P10 compared with control, which was rescued by vit E supplementation (n = 3 per group). *C*, there was no significant difference among the three groups in hydroxy PE-PUFAs-OH (n = 3 per group). *D–F*, there was no significant change in the compositions of PC-PUFAs, PC-PUFAs-OOH, or PC-PUFAs-OH among control, mGPx4 KO, and vit E-supplemented mGPx4 KO mice (n = 3 per group). *$p < 0.05$, **$p < 0.01$ (KO with vitamin E *versus* KO), #$p < 0.05$ (KO *versus* control) using one-way ANOVA and the Tukey–Kramer post hoc test. DHA, docosahexaenoic acid; mGPx4, mitochondrial isoform of GPx4; PC, phosphatidylcholine; PE, phosphatidylethanolamine; PUFA, polyunsaturated fatty acid; vit E, vitamin E.

Based on observations by TEM, the mitochondria in mGPx4 KO photoreceptors were larger in size and fewer in number, which suggests that mitochondria were inclined toward fusion rather than fission. When evaluating the expressions of fusion/fission proteins, we observed an upregulation of MFN2 in the mGPx4 KO retina. MFN2 locates at the outer mitochondrial membrane and endoplasmic reticulum (ER), and it plays key roles in mitochondrial fusion, modulating ER stress, and interactions between the ER and mitochondria. A recent study suggested that MSN1/2 mediates mitochondrial fusion and lipid peroxidation and found that MFN1/2 depletion reduced the sensitivity of pancreatic cancer cells to erastin-induced

ferroptosis (39). Another study reported a role of MFN2 to mediate lipid peroxidation and arsenic-induced ferroptotic cell death in a hepatocyte cell line (40). In addition, the other study reported that relative lipid peroxidation is associated with mitochondrial fusion phenotypes (41). Based on these studies, we speculated in this study that the increased levels of MFN2 in mGPx4 KO retina might have mediated not only mitochondrial fusion but also lipid peroxidation and photoreceptor death. The other hypothesis is that mitochondrial fusion in mGPx4 KO mouse retinas might be influenced by the decrease of PE (22:6/22:6), a unique molecular species of PE-containing double unsaturated fatty acid, and the increase of its oxidative products, PE-OOH (22:6/22:6-OOH) (Fig. 6), which needs further investigations.

In conclusion, the current study addressed the isoform-specific roles of GPx4 in the mitochondria for photoreceptor development and survival. mGPx4 is indispensable for cone photoreceptors at the early stage of their development. In contrast, rod photoreceptors can mature without mGPx4, although they degenerate gradually afterward. Consequently, the different effects of mGPx4 KO on cone and rod photoreceptors produce a retinal degeneration phenotype resembling human cone–rod dystrophy.

Experimental procedures

Construction of mGPx4 KO transgenic vector

To construct the mGPx4 KO transgenic gene (Tg(mGPx4KO), Fig. S1*A*), the approximate 5 kbp upstream regulatory region, E1a, and E1b regions (EcoRI/BamHI; Fig. S1*A*) containing a mutation in the first start codon for mitochondrial GPx4 from ATG to TTG, E1b and EII regions (BamHI/EcoRI; Fig. S1*A*), and EII-VII and 1 kbp downstream region (EcoRI/ApaI; Fig. S1*A*) were separately prepared from our previously cloned mouse GPx4 gene (5, 9) and inserted into Bluescript SK+. To identify mRNA for GPx4 transcribed from transgene, we replaced the NheI site located after the stop codon in the GPx4 gene with BamHI site (Fig. S1*A*). A transgenic screening vector pTG2, containing a 5′-end marker from part of the hygromycin complementary DNA (cDNA) (250 to 660 bp site), a marker sequence (L) for Tg(mGPx4 KO) transgenic gene screening sites (from the cGPx cDNA [27 to 272 bp site; 5′-GGCACAGTCCACCGTCTATG-3′/5′-AGAATCTCTTCATTCTTGCC-3′], and Luciferase cDNA [48 to 373 bp site; 5′-GCTGGAAGATGGAACCGCT-3′/5′-CGGTAGGCTGCGAAATGCC-3′]) was constructed between two SalI sites in Bluescript SK+. Mouse genomic DNA containing a mutation at the start codon for mitochondrial GPx4 digested with SalI was inserted into the XhoI site of the TG2 vector. Finally, the mGPx4 KO transgenic gene, Tg(mGPx4 KO), was excised with SalI from pTG2 vector and purified.

Animals

All procedures were followed by the Association for Research in Vision and Opthalmology Statement for the Use of Animals in Ophthalmic and Vision Research. All experiments were approved by the Institutional Animal Research Committee of the University of Tokyo and Kitasato University. Mice were housed in cages with food and water and subjected to a standard 12 h light/dark cycle at 22 °C.

mGPx4 KO mice were generated by transgenic rescue methods as previously described (12). Briefly, the Tg(mGPx4 KO) transgenic gene was injected into fertilized eggs derived from bromodomain factor 1 parents. Transgenic mGPx4 KO mice ($GPx4^{+/+}$::$GPx4^{tg(mGPx4\ KO)/-}$) were generated by standard methods. To facilitate genotyping of the transgenic mice, the following primer pair specific to Tg (mGPx4 KO) was used: PHGP BAMS/LOXSCR-AS, 5′-CTCTAGGGATCCTAGCCCTACAAGTGTGTCCC-3′/5′-CTTGCCATTCTCCTGATGTCCGAAC-3′. Tg(mGPx4 KO) mice were then mated with GPx4 heterozygous ($GPx4^{+/-}$) mice that we had established previously (2). Furthermore, Tg(mGPx4 KO) transgenic GPx4 heterozygous mice ($GPx4^{+/-}$::$GPx4^{tg(mGPx4\ KO)/-}$) were mated with GPx4 heterozygous mice ($GPx4^{+/-}$) to obtain Tg(mGPx4 KO) transgene-rescued GPx4 KO mice ($GPx4^{-/-}$::$GPx4^{tg(mGPx4\ KO)/-}$). Three primer pairs were used for genotyping (Fig. S1*B*); one specific for Tg(mGPx4 KO) as described previously; one specific for WT allele (103/G1R, 5′-CTGCGTGGTGAAGCGCTAT-3′/5′-AGCGTCATCCACTTCAGCC-3′); and one specific for KO allele (NEOF3/G1R, 5′-CGATGCCTGCTTGCCGAAT-3′/5′-AGCGTCATCCACTT-CAGCC-3′). After several generations, a mouse colony with homozygous transgenic mGPx4 KO alleles without endogenous GPx4 alleles ($GPx4^{-/-}$::$GPx4^{tg(mGPx4\ KO)/tg(mGPx4\ KO)}$) was established and referred to as mGPx4 KO mice. Since mGPx4 KO mice show male infertility, the mouse line was maintained by crossbreeding female mGPx4 KO ($GPx4^{-/-}$::$GPx4^{tg(mGPx4\ KO)/tg(mGPx4\ KO)}$) mice with male $GPx4^{+/-}$::$GPx4^{tg(mGPx4\ KO)/tg(mGPx4\ KO)}$ mice. Offspring genotyped as $GPx4^{+/-}$::$GPx4^{tg(mGPx4\ KO)/tg(mGPx4\ KO)}$ were used as control mice to be compared with their mGPx4 KO littermate. mGPx4 KO and control mice used in this study were from a mixed genetic background with contributions of TT2, Institute of Cancer Research, and bromodomain factor strains for the experiments on male infertility and additional C57BL/6J background for the retina-related experiments. To investigate the reproductive capacities of mGPx4 KO and control mice, one male mouse was mated with two Institute of Cancer Research females for 2 weeks. Female mice were checked for vaginal plugs each morning, and litter sizes were recorded on delivery, after three successive matings. Vit E-enriched diet was made of the standard rodent diet CE-2 (CLEA Japan) enriched with DL-α tocopheryl acetate (1000 IU/kg).

Evaluation of epididymal spermatozoa and histological analysis of testis

The cauda region of the epididymis obtained from ∼12-week-old mice was placed in TYH medium (Mitsubishi Chemical Medience Corp) and gently minced with a surgical blade and incubated at 37 °C for 1 h. Spermatozoa were examined for structure, the number, and mitochondrial membrane potential. To measure mitochondrial membrane potential, spermatozoa were examined by monitoring the

fluorescence of $DiOC_6$ (Molecular Probes). 1×10^5 spermatozoa were incubated for 1 h and then stained with 10 μg/ml DiOC6, 1 μg/ml Hoechst 33258 for 20 min, and washed with PBS. The stained sperm cells were dropped onto glass slides. Fluorescence because of $DiOC_6$ and Hoechst in spermatozoa was monitored and photographed with a fluorescence microscope (BIOZERO, BZ-8000; Keyence). Testis from WT mice and mGPx4 KO mice was fixed in Bouin's solution and embedded in paraffin, and sections were stained with hematoxylin and eosin.

Immunohistochemistry and TUNEL assay

For frozen sections, enucleated eyeballs were fixed in 4% paraformaldehyde for 2 h and put in 30% sucrose in 4 °C overnight. Cryosections were made at −20 °C (thickness, 10 μm). Slides were blocked by Blocking One Histo (Nacalai Tesque, Inc) for 10 min. Then they were incubated with primary antibodies at 4 °C overnight and with secondary antibodies for 1 h at room temperature. The sections were then coverslipped with mounting medium. The following primary antibodies were used; antirhodopsin (1:100 dilution; Santa Cruz Biotechnology; catalog no.: sc-57432), anti-Rxr-γ (1:800 dilution; Santa Cruz Biotechnology; catalog no.: sc-365252), anticone arrestin (1:1000 dilution; Sigma–Aldrich; catalog no.: AB15282), anti-S opsin (1:1000 dilution; Millipore; catalog no.: AB5407), and anti–cleaved-caspase-3 (1:800 dilution; Cell Signaling; catalog no.: 9664), and GPx4 (1:1000 dilution) (42). Alexa Fluor 488 (1:500 dilution; Thermo Fisher Scientific; catalog nos.: A-11209 and A-11008) and 647 (1:250 dilution; Abcam; catalog no.: ab150115)-conjugated secondary antibodies were used for secondary antibodies. For staining nuclei, 4,6-diamidino-2-phenylindole (Sigma–Aldrich) was used. Fluorescent conjugates of PNA lectin (Invitrogen; catalog no.: L21409) were used to label cone cells. ApopTag Peroxidase *In Situ* Apoptosis Detection Kit (Sigma–Aldrich) was used for labeling DNA-strand breaks according to the manufacturer's protocol.

For immunohistochemistry of RPE flatmounts, enucleated eyeballs were fixed in 4% paraformaldehyde for 1 h. RPE-eyecups were flat mounted and blocked by Blocking One Histo for 1 h. Then they were incubated overnight at 4 °C with primary antibody (anti-ZO-1; 1:200 dilution; Thermo Fisher Scientific; catalog no.: 61-7300). After washing RPE flatmounts, they were incubated for 1 h with a secondary antibody (Alexa Fluor 488-conjugated secondary antibody; 1:250 dilution; Thermo Fisher Scientific; catalog no.: A-11008) and coverslipped with mounting medium.

TEM and quantification of number and area of mitochondria

The suspension of epididymal spermatozoa was placed on silane-coated glass and fixed in a solution of 2.5% glutaraldehyde in 0.1 M phosphate buffer. The sample was postfixed in a solution of 1% OsO_4 in 0.1 M phosphate buffer, dehydrated through a graded series of ethanol solutions, and embedded in Epon 812. Ultrathin sections were double stained with uranyl acetate and lead citrate and then examined by TEM (Hitachi H-7100) operated at 75 kV. We examined 10 longitudinal profiles of sperm in 10 longitudinal sections of the midpiece.

Mouse eyes were enucleated and fixed in 2% paraformaldehyde at 4 °C overnight. The sections were made with 1.5 μm thickness and stained with 0.5% toluidine blue. The images were captured by a transmission electron microscope (100 kV, model JEM-1400Plus; JEOL Ltd) *via* a charge-coupled device camera (EM-14830RUBY2; JEOL Ltd). To compare the number of mitochondria, we counted the number of mitochondria of four sections of each group.

Subcellular fractionation

Cytosolic, mitochondrial, and nuclear fractions were prepared from WT, control, and mGPx4 KO retinas and testes. The tissues were dissected and homogenized in lysis buffer (0.25 M sucrose, 3 mM imidazole, and 1 mM EDTA-2Na) with 1% protease inhibitor (abcam; catalog no.: ab65320). The lysate was centrifugated at 2000 rpm for 10 min at 4 °C, and the supernatant was collected as postnuclear fraction. The pellet was resuspended with a Nuclear Extract kit (ACTIVE MOTIF 40010) for 30 min at 4 °C, and the solution was centrifugated at 14,000*g* for 10 min at 4 °C. The supernatant was used as nuclear fraction. The postnuclear fraction was centrifugated at 8000 rpm for 10 min at 4 °C. After centrifugation, the supernatant was collected as cytosol fraction. The pellet was resuspended with radioimmunoprecipitation assay buffer as mitochondrial fraction. Protein amounts in cytosolic and mitochondrial fractions were determined using the bicinchoninic acid assay (Thermo Fisher Scientific; catalog no.: 23227).

Western blotting

Samples were homogenized in radioimmunoprecipitation assay buffer (Thermo Fisher Scientific). Proteins were separated using 4 to 12% or 12% polyacrylamide gels and transferred to a polyvinylidene difluoride membrane (Bio-Rad Laboratories). The membrane was blocked by Blocking One (Nacalai Tesque, Inc) for 10 min and then was incubated with primary antibody overnight at 4 °C. The images of membrane were captured by an ImageQuant LAS 4000 mini-camera system (GE Healthcare). The following primary antibodies were used; anti-GAPDH (1:10,000 dilution; Wako Pure Chemical Industries; catalog no.: 016-25523), anti-SOD1 (1:1000 dilution; Santa Cruz; catalog no.: sc-27104), anti-TIM23 (1:1000 dilution; Proteintech; catalog no.: 11123-1-AP), anti-VDAC (Porin31 HL; 1:1000 dilution; Calbiochem), anti-PCNA (1:1000 dilution; BD Biosciences Pharmingen; catalog no.: 610,664), anti-GPx4 (1:5000 dilution) (42), antiacrolein (1:1000 dilution; NOF; catalog no.: N213320), anti-MFN1 (1:100 dilution; Santa Cruz Biotechnology; catalog no.: sc-166644) anti-MFN2 (1:1000 dilution; Abcam; catalog no.: ab56889), anti–optic atrophy 1 (1:1000 dilution; BD Transduction Laboratories; catalog no.: 612606), anti-phospho-DRP1 (Ser637) (1:1000 dilution; Cell Signaling; catalog no.: 4867), and anti–phospho-DRP1 (Ser616) (1:1000 dilution; Cell Signaling; catalog no.: 3455). For secondary antibodies, horseradish peroxidase–linked antibody (Cell Signaling; catalog nos.: 7074 and 7076) were used. The band intensities were quantified using ImageJ software (version 1.53; National Institutes of Health).

ERG

The ERG was recorded using a LS–W (Mayo) and analyzed using Scope 3 software (ADInstruments) for scotopic condition and LabChart 8 software (ADInstruments) for photopic condition. The scotopic ERG was recorded in 7-week-old mice, and the photopic ERG was recorded in 4-week-old mice. Scotopic ERG was recorded after 12 h of dark adaptation. The flash intensities ranged from 1.5 to 4500 cdms/m^2. Data from three trials were averaged for single-flash responses. Photopic ERGs were recorded after light adaptation. The flash intensities ranged from 1778 to 22,330 cdms/m^2 with a background illumination of 35 cd/m^2. Data from 32 trials were averaged for single-flash responses.

Phospholipid analysis by LC–MS

The retinas were isolated from enucleated eyes and stored at −80 °C immediately. The concentrations of PE, PE-OOH, PE-OH, PC, PC-OOH, and PC-OH in each sample were measured using QTRAP 4500 quadrupole linear ion trap hybrid mass spectrometer (AB Sciex) coupled to a Nexera XR high-performance liquid chromatography system (Shimadzu Co), as previously described (19, 43).

Statistics

All statistical analyses were performed using EZR (44) (Saitama Medical Center, Jichi Medical University), which is based on R 4.0.3 (The R Foundation for Statistical Computing). EZR is a modified version of R commander designed to add statistical functions frequently used in biostatistics. Data are presented as a mean value with standard error. Student's *t* test was performed to compare two groups. For comparisons among three groups, one-way ANOVA was conducted, followed by Tukey's post hoc test. *p* Values less than 0.05 were considered to be statistically significant.

Data availability

All data are contained within the manuscript.

Supporting information—This article contains supporting information.

Acknowledgments—We thank Tajima-Iwamoto and Matsubara (School of Pharmaceutical Sciences, Kitasato University) for generation of mGPx4KO mice, Ichinose (Instrumental Analysis Research Center, School of Medicine, Tokyo Medical and Dental University) for TEM analysis for spermatozoa, and Tsuhako (Institute of Medical Science, the University of Tokyo) for supporting ERG experiments. This work was supported by Kitasato University Research Grant for Young Researcher and Japan Agency for Medical Research and Development (AMED) (grant numbers: JP20gm0910013 and JP21gm0910013) and Japan Society for the Promotion of Science KAKENHI (grant number: JP19K18901).

Author contributions—H. I. and T. U. conceptualization; T. K., S. W., M. A., H. I., and T. U. methodology; K. A. formal analysis; K. A., R. I., M. M., R. T., S. Y., and T. U. investigation; T. K. and H. I. resources; K. A. writing–original draft; T. S., S. W., M. A., H. I., and T. U. writing–review & editing; T. S., S. W., M. A., H. I., and T. U. supervision; T. U. project administration; H. I. and T. U. funding acquisition.

Conflict of interest—The authors declare that they have no conflicts of interest with the contents of this article.

Abbreviations—The abbreviations used are: cDNA, complementary DNA; cGPx4, cytosolic isoform of GPx4; DHA, docosahexaenoic acid; DRP1, dynamin-related protein 1; ER, endoplasmic reticulum; ERG, electroretinogram; GPx4, glutathione peroxidase 4; MFN1, mitofusion 1; MFN2, mitofusion 2; mGPx4, mitochondrial isoform of GPx4; nGPx4, nucleolar isoform of GPx4; ONL, outer nuclear layer; PC, phosphatidylcholine; PE, phosphatidylethanolamine; PNA, peanut agglutinin; PUFA, polyunsaturated fatty acid; RPE, retinal pigment epithelium; TEM, transmission electron microscopy; vit E, vitamin E.

References

1. Yang, W. S., SriRamaratnam, R., Welsch, M. E., Shimada, K., Skouta, R., Viswanathan, V. S., Cheah, J. H., Clemons, P. A., Shamji, A. F., Clish, C. B., Brown, L. M., Girotti, A. W., Cornish, V. W., Schreiber, S. L., and Stockwell, B. R. (2014) Regulation of ferroptotic cancer cell death by GPX4. *Cell* **156**, 317–331
2. Imai, H., Hirao, F., Sakamoto, T., Sekine, K., Mizukura, Y., Saito, M., Kitamoto, T., Hayasaka, M., Hanaoka, K., and Nakagawa, Y. (2003) Early embryonic lethality caused by targeted disruption of the mouse PHGPx gene. *Biochem. Biophys. Res. Commun.* **305**, 278–286
3. Imai, H., Matsuoka, M., Kumagai, T., Sakamoto, T., and Koumura, T. (2016) Lipid peroxidation-dependent cell death regulated by GPx4 and ferroptosis. In: Nagata, S., Nakano, H., eds.**, 403**. *Apoptotic and Non-apoptotic Cell Death*, Current Topics in Microbiology and Immunology, Springer International Publishing, Cham: 143–170
4. Carlson, B. A., Tobe, R., Yefremova, E., Tsuji, P. A., Hoffmann, V. J., Schweizer, U., Gladyshev, V. N., Hatfield, D. L., and Conrad, M. (2016) Glutathione peroxidase 4 and vitamin E cooperatively prevent hepatocellular degeneration. *Redox Biol.* **9**, 22–31
5. Imai, H., Hakkaku, N., Iwamoto, R., Suzuki, J., Suzuki, T., Tajima, Y., Konishi, K., Minami, S., Ichinose, S., Ishizaka, K., Shioda, S., Arata, S., Nishimura, M., Naito, S., and Nakagawa, Y. (2009) Depletion of selenoprotein GPx4 in spermatocytes causes male infertility in mice. *J. Biol. Chem.* **284**, 32522–32532
6. Friedmann Angeli, J. P., Schneider, M., Proneth, B., Tyurina, Y. Y., Tyurin, V. A., Hammond, V. J., Herbach, N., Aichler, M., Walch, A., Eggenhofer, E., Basavarajappa, D., Rådmark, O., Kobayashi, S., Seibt, T., Beck, H., *et al.* (2014) Inactivation of the ferroptosis regulator Gpx4 triggers acute renal failure in mice. *Nat. Cell Biol.* **16**, 1180–1191
7. Arai, M., Imai, H., Sumi, D., Imanaka, T., Takano, T., Chiba, N., and Nakagawa, Y. (1996) Import into mitochondria of phospholipid hydroperoxide glutathione peroxidase requires a leader sequence. *Biochem. Biophys. Res. Commun.* **227**, 433–439
8. Nakamura, T., Imai, H., Tsunashima, N., and Nakagawa, Y. (2003) Molecular cloning and functional expression of nucleolar phospholipid hydroperoxide glutathione peroxidase in mammalian cells. *Biochem. Biophys. Res. Commun.* **311**, 139–148
9. Imai, H., Saito, M., Kirai, N., Hasegawa, J., Konishi, K., Hattori, H., Nishimura, M., Naito, S., and Nakagawa, Y. (2006) Identification of the positive regulatory and distinct core regions of promoters, and transcriptional regulation in three types of mouse phospholipid hydroperoxide glutathione peroxidase. *J. Biochem. (Tokyo)* **140**, 573–590
10. Schneider, M., Förster, H., Boersma, A., Seiler, A., Wehnes, H., Sinowatz, F., Neumüller, C., Deutsch, M. J., Walch, A., Hrabé de Angelis, M., Wurst, W., Ursini, F., Roveri, A., Maleszewski, M., Maiorino, M., *et al.*

(2009) Mitochondrial glutathione peroxidase 4 disruption causes male infertility. *FASEB J. Off. Publ. Fed. Am. Soc. Exp. Biol.* **23**, 3233–3242
11. Liang, H., Yoo, S.-E., Na, R., Walter, C. A., Richardson, A., and Ran, Q. (2009) Short form glutathione peroxidase 4 is the essential isoform required for survival and somatic mitochondrial functions. *J. Biol. Chem.* **284**, 30836–30844
12. Imai, H. (2010) New strategy of functional analysis of PHGPx knockout mice model using transgenic rescue method and Cre-LoxP system. *J. Clin. Biochem. Nutr.* **46**, 1–13
13. Fliesler, S. J., and Anderson, R. E. (1983) Chemistry and metabolism of lipids in the vertebrate retina. *Prog. Lipid Res.* **22**, 79–131
14. SanGiovanni, J. P., and Chew, E. Y. (2005) The role of omega-3 long-chain polyunsaturated fatty acids in health and disease of the retina. *Prog. Retin. Eye Res.* **24**, 87–138
15. Wong-Riley, M. T. T. (2010) Energy metabolism of the visual system. *Eye Brain* **2**, 99–116
16. Ueta, T., Inoue, T., Furukawa, T., Tamaki, Y., Nakagawa, Y., Imai, H., and Yanagi, Y. (2012) Glutathione peroxidase 4 is required for maturation of photoreceptor cells. *J. Biol. Chem.* **287**, 7675–7682
17. Chen, L., Hambright, W. S., Na, R., and Ran, Q. (2015) Ablation of the ferroptosis inhibitor glutathione peroxidase 4 in neurons results in rapid motor neuron degeneration and paralysis. *J. Biol. Chem.* **290**, 28097–28106
18. Yang, W. S., and Stockwell, B. R. (2008) Synthetic lethal screening identifies compounds activating iron-dependent, nonapoptotic cell death in oncogenic-RAS-harboring cancer cells. *Chem. Biol.* **15**, 234–245
19. Yoshida, M., Minagawa, S., Araya, J., Sakamoto, T., Hara, H., Tsubouchi, K., Hosaka, Y., Ichikawa, A., Saito, N., Kadota, T., Sato, N., Kurita, Y., Kobayashi, K., Ito, S., Utsumi, H., *et al.* (2019) Involvement of cigarette smoke-induced epithelial cell ferroptosis in COPD pathogenesis. *Nat. Commun.* **10**, 3145
20. Tsubouchi, K., Araya, J., Yoshida, M., Sakamoto, T., Koumura, T., Minagawa, S., Hara, H., Hosaka, Y., Ichikawa, A., Saito, N., Kadota, T., Kurita, Y., Kobayashi, K., Ito, S., Fujita, Y., *et al.* (2019) Involvement of GPx4-regulated lipid peroxidation in idiopathic pulmonary fibrosis pathogenesis. *J. Immunol. Baltim. Md.* **203**, 2076–2087
21. Ni, Y., and Eng, C. (2012) Vitamin E protects against lipid peroxidation and rescues tumorigenic phenotypes in cowden/cowden-like patient-derived lymphoblast cells with germline SDHx variants. *Clin. Cancer Res.* **18**, 4954–4961
22. Meschede, I. P., Ovenden, N. C., Seabra, M. C., Futter, C. E., Votruba, M., Cheetham, M. E., and Burgoyne, T. (2020) Symmetric arrangement of mitochondria:plasma membrane contacts between adjacent photoreceptor cells regulated by Opa1. *Proc. Natl. Acad. Sci. U. S. A.* **117**, 15684–15693
23. Elmore, S. (2007) Apoptosis: A review of programmed cell death. *Toxicol. Pathol.* **35**, 495–516
24. Basu Ball, W., Neff, J. K., and Gohil, V. M. (2018) The role of nonbilayer phospholipids in mitochondrial structure and function. *FEBS Lett.* **592**, 1273–1290
25. Lu, L., Oveson, B. C., Jo, Y., Lauer, T. W., Usui, S., Komeima, K., Xie, B., and Campochiaro, P. A. (2009) Increased expression of glutathione peroxidase 4 strongly protects retina from oxidative damage. *Antioxid. Redox Signal.* **11**, 715–724
26. Shen, J., Yang, X., Dong, A., Petters, R. M., Peng, Y.-W., Wong, F., and Campochiaro, P. A. (2005) Oxidative damage is a potential cause of cone cell death in retinitis pigmentosa. *J. Cell. Physiol.* **203**, 457–464
27. Didenco, S., Gillingham, M. B., Go, M. D., Leonard, S. W., Traber, M. G., and McEvoy, C. T. (2011) Increased vitamin E intake is associated with higher alpha-tocopherol concentration in the maternal circulation but higher alpha-carboxyethyl hydroxychroman concentration in the fetal circulation. *Am. J. Clin. Nutr.* **93**, 368–373
28. Brzezinski, J. A., and Reh, T. A. (2015) Photoreceptor cell fate specification in vertebrates. *Dev. Camb. Engl.* **142**, 3263–3273
29. Ursini, F., Heim, S., Kiess, M., Maiorino, M., Roveri, A., Wissing, J., and Flohé, L. (1999) Dual function of the selenoprotein PHGPx during sperm maturation. *Science* **285**, 1393–1396
30. Shindou, H., Koso, H., Sasaki, J., Nakanishi, H., Sagara, H., Nakagawa, K. M., Takahashi, Y., Hishikawa, D., Iizuka-Hishikawa, Y., Tokumasu, F., Noguchi, H., Watanabe, S., Sasaki, T., and Shimizu, T. (2017) Docosahexaenoic acid preserves visual function by maintaining correct disc morphology in retinal photoreceptor cells. *J. Biol. Chem.* **292**, 12054–12064
31. Bazan, N. G., Molina, M. F., and Gordon, W. C. (2011) Docosahexaenoic acid signalolipidomics in nutrition: Significance in aging, neuroinflammation, macular degeneration, Alzheimer's, and other neurodegenerative diseases. *Annu. Rev. Nutr.* **31**, 321–351
32. Conrad, M., Kagan, V. E., Bayir, H., Pagnussat, G. C., Head, B., Traber, M. G., and Stockwell, B. R. (2018) Regulation of lipid peroxidation and ferroptosis in diverse species. *Genes Dev.* **32**, 602–619
33. DeHart, D. N., Lemasters, J. J., and Maldonado, E. N. (2018) Erastin-like anti-warburg agents prevent mitochondrial depolarization induced by free tubulin and decrease lactate formation in cancer cells. *SLAS Discov. Adv. Life Sci. R. D.* **23**, 23–33
34. Wang, H., Liu, C., Zhao, Y., and Gao, G. (2020) Mitochondria regulation in ferroptosis. *Eur. J. Cell Biol.* **99**, 151058
35. Dong, H., Qiang, Z., Chai, D., Peng, J., Xia, Y., Hu, R., and Jiang, H. (2020) Nrf2 inhibits ferroptosis and protects against acute lung injury due to intestinal ischemia reperfusion *via* regulating SLC7A11 and HO-1. *Aging* **12**, 12943–12959
36. Stockwell, B. R., Friedmann Angeli, J. P., Bayir, H., Bush, A. I., Conrad, M., Dixon, S. J., Fulda, S., Gascón, S., Hatzios, S. K., Kagan, V. E., Noel, K., Jiang, X., Linkermann, A., Murphy, M. E., Overholtzer, M., *et al.* (2017) Ferroptosis: A regulated cell death nexus linking metabolism, redox biology, and disease. *Cell* **171**, 273–285
37. Imai, H., and Nakagawa, Y. (2003) Biological significance of phospholipid hydroperoxide glutathione peroxidase (PHGPx, GPx4) in mammalian cells. *Free Radic. Biol. Med.* **34**, 145–169
38. Nomura, K., Imai, H., Koumura, T., Arai, M., and Nakagawa, Y. (1999) Mitochondrial phospholipid hydroperoxide glutathione peroxidase suppresses apoptosis mediated by a mitochondrial death pathway. *J. Biol. Chem.* **274**, 29294–29302
39. Li, C., Liu, J., Hou, W., Kang, R., and Tang, D. (2021) STING1 promotes ferroptosis through MFN1/2-dependent mitochondrial fusion. *Front. Cell Dev. Biol.* **9**, 698679
40. Wei, S., Qiu, T., Wang, N., Yao, X., Jiang, L., Jia, X., Tao, Y., Zhang, J., Zhu, Y., Yang, G., Liu, X., Liu, S., and Sun, X. (2020) Ferroptosis mediated by the interaction between Mfn2 and IREα promotes arsenic-induced nonalcoholic steatohepatitis. *Environ. Res.* **188**, 109824
41. Castro-Sepulveda, M., Jannas-Vela, S., Fernández-Verdejo, R., Ávalos-Allele, D., Tapia, G., Villagrán, C., Quezada, N., and Zbinden-Foncea, H. (2020) Relative lipid oxidation associates directly with mitochondrial fusion phenotype and mitochondria-sarcoplasmic reticulum interactions in human skeletal muscle. *Am. J. Physiol.-Endocrinol. Metab.* **318**, E848–E855
42. Imai, H., Suzuki, K., Ishizaka, K., Ichinose, S., Oshima, H., Okayasu, I., Emoto, K., Umeda, M., and Nakagawa, Y. (2001) Failure of the expression of phospholipid hydroperoxide glutathione peroxidase in the spermatozoa of human infertile Males1. *Biol. Reprod.* **64**, 674–683
43. Sakamoto, T., Maebayashi, K., Tsunoda, Y., and Imai, H. (2020) Inhibition of lipid peroxidation during the reproductive period extends the lifespan of Caenorhabditis elegans. *J. Clin. Biochem. Nutr.* **66**, 116–123
44. Kanda, Y. (2013) Investigation of the freely available easy-to-use software "EZR" for medical statistics. *Bone Marrow Transpl.* **48**, 452–458